

4,5-Dihydropyrazole derivatives containing oxygen-bearing heterocycles as potential telomerase inhibitors with anticancer activity

 Cite this: *RSC Adv.*, 2014, 4, 23904

 Yin Luo,^{†a} Yang Zhou,^{†a} Jie Fu^b and Hai-Liang Zhu^{*a}

Telomere and telomerase were closely related to the occurrence and development of some cancers. After the key active site of telomerase was identified, to enhance the ability of dihydropyrazole derivatives to inhibit telomerase, we designed a series of novel 4,5-dihydropyrazole derivatives containing heterocyclic oxygen moiety based on previous studies. The telomerase inhibition assay showed that compound **10a** displayed the most potent inhibitory activity with an IC_{50} value of 0.6 μ M for telomerase. The antiproliferative assay showed that **10a** exhibited high activity against human gastric cancer cell SGC-7901 with an IC_{50} value of 10.95 ± 0.60 μ M. Flow cytometric analysis and western blot results showed that **10a** induced both apoptosis and autophagy. A docking simulation showed that **10a** could bind well to the active site of telomerase and act as a telomerase inhibitor. The 3D-QSAR model was also built to provide a more pharmacological understanding that could be used to design new agents with more potent telomerase inhibitory activity.

Received 13th March 2014

Accepted 5th May 2014

DOI: 10.1039/c4ra02200a

www.rsc.org/advances

1 Introduction

To date, to identify efficient anticancer drugs with low toxicity and specific selectivity remains a top priority in the cancer treatment. immortalization of tumor cells is a key characteristic to tumor growth and metastasis. The expression of telomerase in tumor cells is closely related to this proliferation process.¹ Studies have shown that in almost all human malignancies, telomerase had varying degrees of high expression and the activity detection rate was 85–95%, whereas the rate was only 4% in normal tissue around the tumor and in benign lesions.²

Telomerase is active in the early stages of life, when it maintains the telomere length and chromosome integrity in frequently dividing cells. In majority of adult somatic cells, it turns to dormancy.³ However, in cancer cells, telomerase is reactivated to keep the telomere length short in rapidly dividing cells, leading to proliferation.⁴ It was also reported that telomere and telomerase were closely related to the occurrence and development of gastric cancer.⁵ After the discovery of telomerase in cancer cells in 1994, although scientists designed various telomerase inhibitors with some effects, an efficient pilot structure has not yet been identified.^{1,6} The main reason is that conclusive evidence of telomerase as a tumor site-specific

marker has not yet been obtained; thus, inhibitors cannot be accurately designed. Because the American scientist, Andrew J. G., revealed the key active site of telomerase [three-dimensional structure of telomerase reverse transcriptase (TERT) protein catalytic subunit: 3DU6.pdb] in 2008, scientists can now focus on a clear target and try a new molecular designing scheme.^{5,7} At present, although there are some reports about inhibitors for the TERT catalytic subunit of telomerase,^{8,9} there are only few reports about leading compounds due to the late discovery of the crystal structure of 3DU6.

Dihydropyrazoles are extremely important compounds owing to their nitrogen-bearing five-membered heterocyclic ring. Chirality of dihydropyrazole results in greater variability of substituents on the pyrazole ring; thus, molecular conformations with improved biological activity can be obtained. In the past few years, studies showed that compounds with this structure have potential anticancer, antibacterial, antimalarial, analgesic and antiviral effects.^{10–21} Several dihydropyrazole derivatives have also been designed as cannabinoid receptor 1 antagonists, monoamine oxidase inhibitors, and tumor necrosis inhibitors.^{22,23} In an effort to synthesize novel dihydropyrazoles with potential anticancer activity, our group has recently designed some acetyl 4,5-dihydropyrazole derivatives as telomerase inhibitors and tested their anticancer activities. We found that these compounds could be used as targeted anticancer drugs for further study,^{24–26} and the chemical structures of the most active compounds are shown in Fig. 1.

Oxygen-bearing heterocycles, especially 1,3-benzodioxole and 1,4-benzodioxan, have attracted significant attention in chemical, medicinal and pharmaceutical research. These

^aState Key Laboratory of Pharmaceutical Biotechnology, Nanjing University, Nanjing, 210093, People's Republic of China. E-mail: zhuhl@nju.edu.cn; Fax: +86-25-8359 2672; Tel: +86-25-8359 2572

^bEnvironmental Engineering Program, Department of Civil Engineering, Auburn University, Auburn, AL 36839, USA

[†] These two authors equally contributed to this paper.

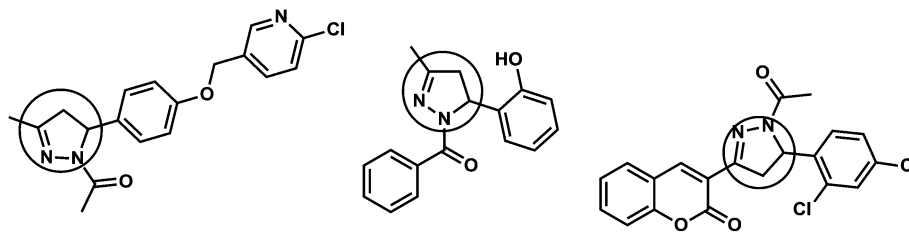


Fig. 1 Chemical structures of some reported dihydropyrazoles as telomerase inhibitors.^{25–27}

structural units were found in a variety of drugs that are used as antihypertensive, anti-inflammatory, antitumor and antimycotic agents.^{27–31}

To extend our research on antiproliferative agents, a series of novel 4,5-dihydropyrazole derivatives containing an oxygen-bearing heterocycle were designed and their enzyme inhibitory activities were tested. The most active compounds were then tested for their activities against SGC-7901 cells and B16-F10 cells. Flow cytometric analysis and a western blot assay were performed to explore probable reaction mechanism. Docking simulations were then performed to position the selected compound into the crystal structure of TERT catalytic subunit to explore a probable binding model. The objectives of the present work are as follows: to synthesize new dihydropyrazole derivatives; to evaluate their telomerase inhibitory activities; to test their anti-cancer activities; to explore the reaction mechanism of the most active compounds and to investigate the interaction between the inhibitor and telomerase using a docking study.

2 Results and discussion

2.1 Chemistry

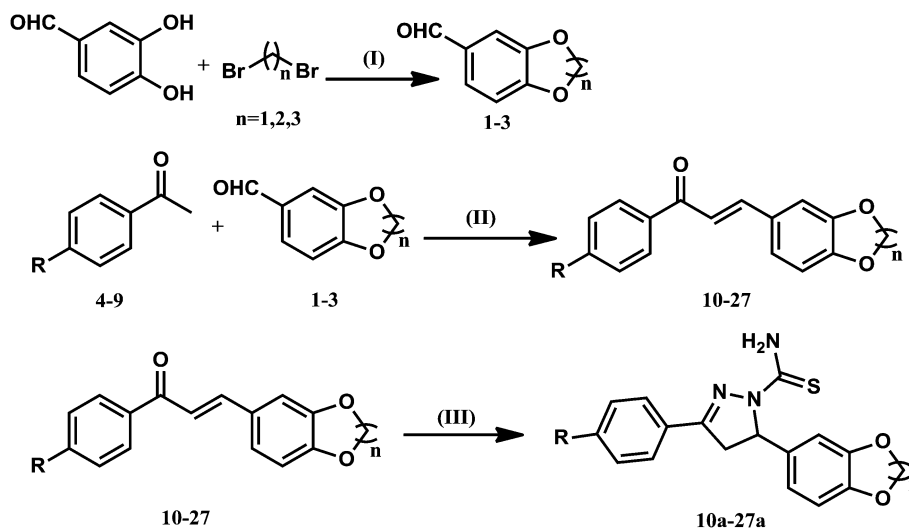
As shown in Scheme 1, compounds 1–3 were synthesized from protocatechualdehyde and dibromomethane, protocatechualdehyde and dibromoethane, and protocatechualdehyde

and dibromopropane with acetone as the solvent in the presence of potassium carbonate. The synthesized compounds were then reacted with substituted acetophenones (4–9) to afford the corresponding chalcone derivatives 10–27. After that, 10–27 were reacted with thiosemicarbazide to synthesize the corresponding dihydropyrazoles 10a–27a. These compounds exhibited satisfactory elementary analyses ($\pm 0.4\%$). ¹H NMR and ESI MS spectra were consistent with the assigned structures.

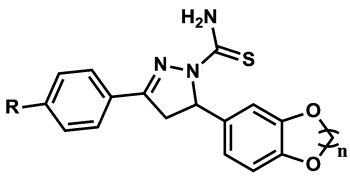
Among these compounds, 22–27 and 10a–27a have been reported for the first time. 10a–15a were dihydropyrazole derivatives containing a 1,3-benzodioxole group prepared from substituted acetophenones, whereas 16a–21a contained a 1,4-benzodioxan group and 22a–27a contained a 1,5-benzodioxepine group. Moreover, the substituents on acetophenones 4–9 were H, F, Cl, Br, CH₃ and OCH₃, respectively, containing both electron-donating and electron-withdrawing groups.

2.2 Biology

2.2.1 Telomerase inhibition assay. All synthesized compounds 10a–27a were evaluated for telomerase inhibitory activity by a modified telomere repeat amplification protocol (TRAP) assay.³² Modified TRAP assay is a useful technique that provides qualitative and quantitative information about small molecules that inhibit telomere elongation.³³ The results are summarized in Table 1. Most of the tested compounds



Scheme 1 Synthetic pathway for preparation of compounds 10a–27a. Reagents: (I) acetone, K₂CO₃, reflux, 24 h; (II) EtOH, KOH (40% aq.), r.t., 2 h; (III) thiosemicarbazide, KOH, ethanol, reflux, 12 h.

Table 1 Inhibitory effects of synthesized compounds against telomerase^a


Compounds	<i>n</i>	R	IC ₅₀ (μM) telomerase
10a	1	OCH ₃	0.6
11a	1	CH ₃	1.9
12a	1	H	8.4
13a	1	Br	13.2
14a	1	Cl	19.3
15a	1	F	25.8
16a	2	OCH ₃	25.6
17a	2	CH ₃	33.4
18a	2	H	38.5
19a	2	Br	42.9
20a	2	Cl	55.7
21a	2	F	No
22a	3	OCH ₃	No
23a	3	CH ₃	No
24a	3	H	No
25a	3	Br	No
26a	3	Cl	No
27a	3	F	No
Ethidium bromide ^b			2.6

^a No indicates that no activity was observed in the concentration range of 0–60 μM. ^b Ethidium bromide is reported as a control. The inhibition constant of ethidium toward telomerase has been reported previously.

displayed good telomerase inhibitory activity and **10a** displayed the best inhibitory activity with an IC₅₀ of 0.6 μM, which was comparable to the reference compound, ethidium bromide.

From the data presented in Table 1, it can be concluded that 4,5-dihydropyrazole derivatives containing 1,3-benzodioxole group (**10a–15a**) displayed better telomerase inhibitory activities, whereas the derivatives containing 1,4-benzodioxan and 1,5-benzodioxepine groups, in general, displayed relatively worse activities.

The results also suggested that the compounds with a 1,3-benzodioxole group (**10a–15a**) and a methoxy group in the R position (**10a** and **16a**) showed better telomerase inhibitory activities than compounds with other substituents. Some compounds in this series were selected for further investigation.

2.2.2 Antiproliferative activity assay. After the enzyme inhibition assay, the most active compounds **10a–17a** were chosen to complete the screening assay studies. Eight compounds were evaluated for their cytotoxic activities against gastric SGC-7901 (human gastric cancer) and B16-F10 (mouse melanoma) cell lines, and the results were summarized in Table 2. Compound **10a** exhibited the best activity against SGC-7901 cells with an IC₅₀ of 10.95 ± 0.60 μM, which is even better than the reference drug 5-fluorouracil (IC₅₀ = 46.35 ± 2.83 μM). All

Table 2 Cytotoxic activity of test compounds against SGC-7901 cell line^a negative control DMSO, no activity

Compounds	IC ₅₀ (μM)	IC ₅₀ (μM)
	SGC-7901	B16-F10
10a	10.95 ± 0.60	28.95 ± 0.84
11a	23.11 ± 0.85	31.59 ± 1.37
12a	21.54 ± 1.32	31.78 ± 1.53
13a	27.87 ± 0.97	35.93 ± 2.11
14a	36.9 ± 1.35	42.85 ± 2.67
15a	38.22 ± 1.78	60.79 ± 2.95
16a	40.22 ± 2.39	39.77 ± 1.42
17a	42.38 ± 2.56	47.12 ± 1.89
5-Fluorouracil ^b	46.35 ± 2.83	21.41 ± 1.76

^a The data represent a mean of three experiments performed in triplicate and are expressed as mean ± SD. ^b Used as a positive control.

the synthesized compounds exhibited worse activity against B16-F10 cells; however, the IC₅₀ values against B16-F10 cells were comparable to the reference drug.

The results were consistent with enzyme inhibition assay results, which showed that compounds with a 1,3-benzodioxole group and a hydrogen atom in the R position showed better activities.

2.2.3 Cell autophagy and apoptosis. Autophagy plays a dichotomous role in mediating cell fate, either protective or destructive, in response to metabolic stress or therapeutic agents.

To explore the antiproliferative reaction mechanism of the most active compounds (**10a–12a**), we assessed their effects on programmed cell death (apoptosis *versus* autophagy) of SGC-7901 cells at a concentration of 3 μM. As shown in Fig. 2, flow

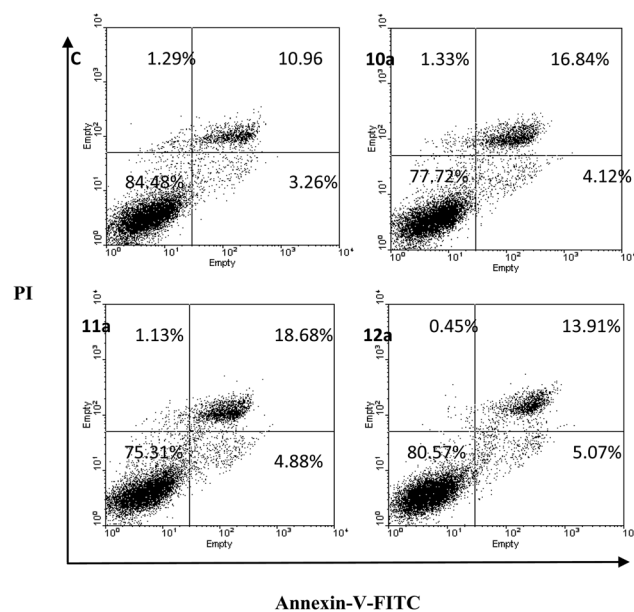


Fig. 2 Apoptosis of compounds **10a**, **11a** and **12a** (3 μM) was analyzed by flow cytometry. The values in the right upper and lower quadrants denote an average value of three independent experiments. C: control.

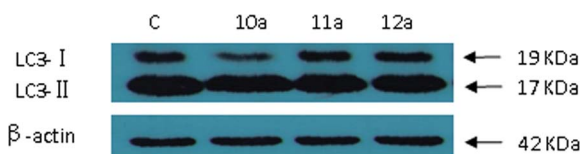


Fig. 3 Autophagy of compounds **10a**, **11a** and **12a** was analyzed using a western blot. LC3-I and LC3-II conversion in SGC-7901 cells after 24 h of treatment.

cytometric analysis indicated some small changes in the induction of apoptosis when compounds **10a**, **11a** and **12a** were tested. Western blot analysis of LC3-I and LC3-II conversion revealed that **10a** and **12a** induced autophagy (Fig. 3). Thus, it could be suggested that **10a** and **12a** might induce both apoptosis and autophagy. This finding suggests that the induction of autophagy and apoptosis was a possible mechanism, by which **10a** mediated its antiproliferative activity.

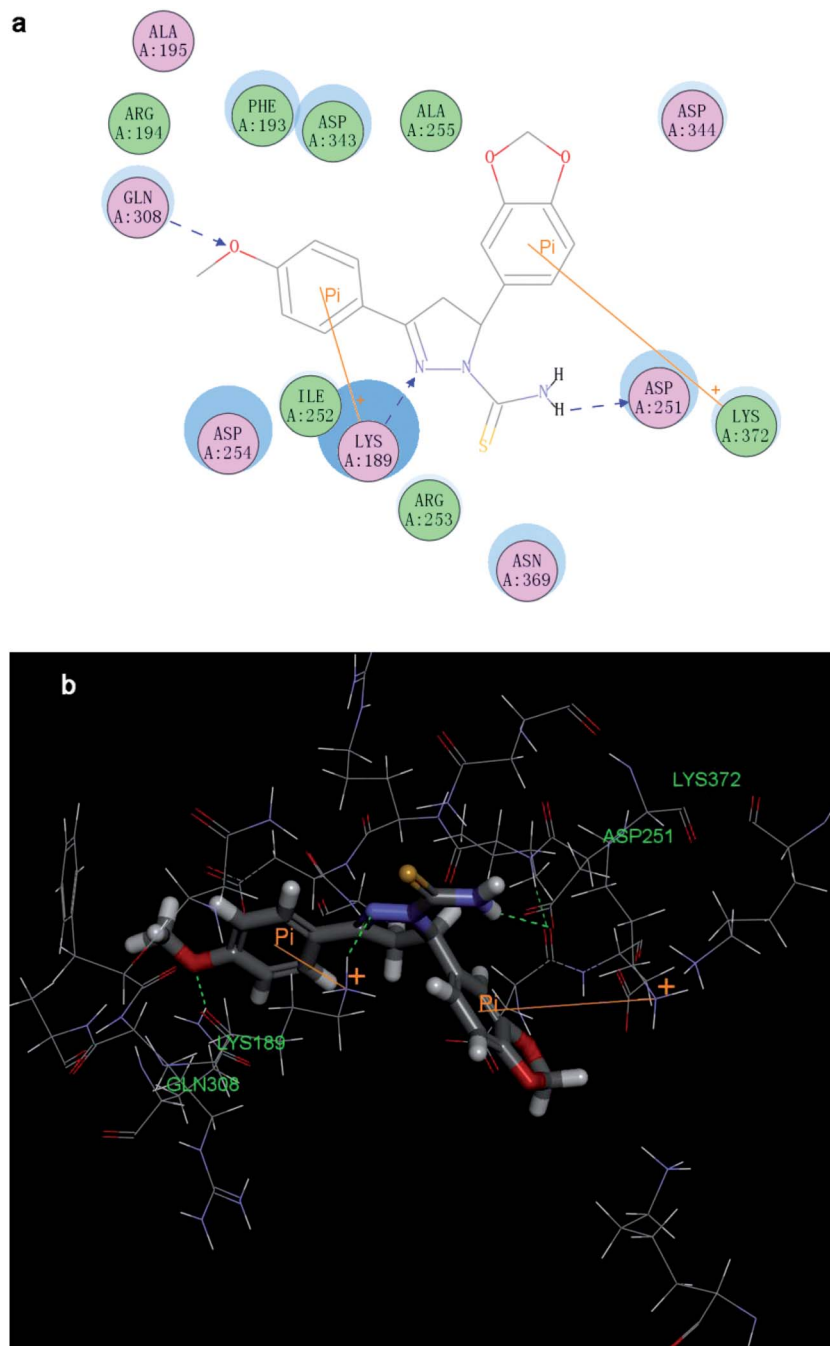


Fig. 4 (a) 2D ligand interaction diagram of compound **10a** (*R*-isomer) with TERT protein catalytic subunit (PDB ID: 3DU6) using the Discovery Studio program; the essential amino acid residues at the binding site are circled. The purple circles show the amino acids that participate in hydrogen bonding, electrostatic or polar interactions and the green circles show the amino acids that participate in the van der Waals interactions. (b) The 3D model structure of compound **10a** binding with the telomerase complex.

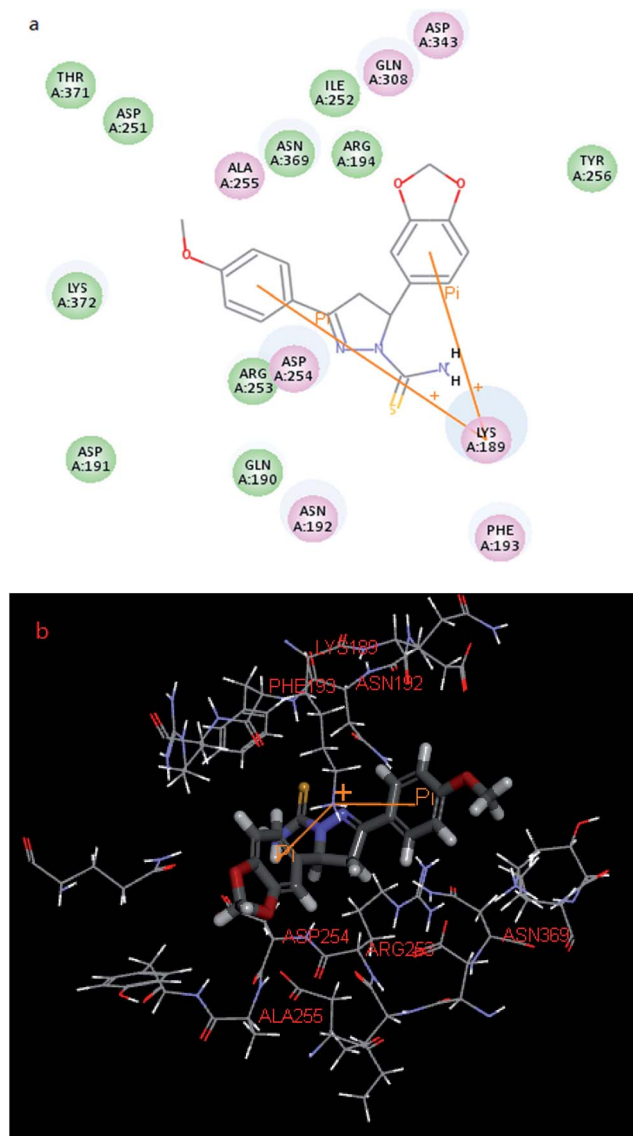


Fig. 5 (a) 2D ligand interaction diagram of compound **10a** (*S*-isomer) with TERT protein catalytic subunit (PDB ID: 3DU6). (b) The 3D model structure of compound **10a** binding with the telomerase complex.

2.3 Molecular docking

In order to explore probable interaction models of the inhibitors in the enzyme active site, molecular docking of **10a** (both the enantiomers were selected) into an active binding site of the telomerase was performed to simulate the binding model derived from the TERT protein catalytic subunit (3DU6.pdb).

All docking runs were applied using the CDOCKER Dock protocol of Discovery Studio 3.5. The binding model of **10a** (*R*-isomer) and telomerase is depicted in Fig. 4. In the binding model, **10a** was nicely bound to the TERT protein catalytic subunit *via* three interaction bonds with a binding energy of $-33.80 \text{ kJ mol}^{-1}$. The visual inspection of **10a** in the active site revealed that three optimal intramolecular hydrogen bonds were observed (N–H \cdots O: angle = 153.49° , distance = 2.2 \AA with the amino hydrogen group of GLN308; N–H \cdots N: angle =

115.31° , distance = 2.3 \AA with the amino hydrogen group of LYS189; N–H \cdots O: angle = 142.38° , distance = 2.2 \AA with the oxygen group of ASP251). Moreover, the end amino cation of LYS189 (distance: 4.1 \AA) exhibited π -cation interaction with one of the benzene rings in **10a**. Furthermore, the end amino of HIS304 exhibited π - π interaction with another benzene ring in compound **10a**. These residues influenced the accessibility of the hydrophobic pocket that flanked the active binding site, and their size could be important in controlling the telomerase selectivity. At the other end of the binding pocket, the sulfur atom of dihydropyrazole ethanethioamide interacted with the residue ARG253, which made the 3D structure more stable.

Fig. 5 shows the binding model of **10a** (*S*-isomer) with telomerase. In this model, **10a** was bound to the TERT protein catalytic subunit by two π -cation interaction bonds with a binding energy of $-32.59 \text{ kJ mol}^{-1}$. This model was less stable compared with the *R*-isomer model.

2.4 3D-QSAR model

In our previous paper, we built a 3D-QSAR model that could be used to predict and guide further drug design.³⁵ In this paper, a new 3D-QSAR model was developed. In order to build a more

Table 3 Experimental and predicted inhibitory activities of compounds by 3D-QSAR models based on active conformations achieved by molecular docking

Compound	Experimental pIC ₅₀	Predicted pIC ₅₀	Residual error
10a	6.22185	4.94834	1.27351
11a	5.72125	5.52509	0.196164
12a	5.07572	5.13092	-0.0552
13a	4.87943	5.01712	-0.13769
14a	4.71444	4.72311	-0.00867
15a	4.58838	4.62442	-0.03604
16a	4.59176	4.55839	0.033368
17a	4.47625	4.64458	-0.16833
19a	4.36754	4.39691	-0.02937
20a	4.25414	4.23813	0.016013
11a^a	5.46852	5.48395	-0.01543
12A	5.13668	5.18814	-0.05146
13A	5.17393	5.12611	0.04782
14A	5.20761	5.19633	0.011283
15A	5.88606	4.95256	0.933502
16A	6.04576	6.08272	-0.03696
17A	5.06048	5.06329	-0.00281
18A	4.73283	4.53594	0.196886
19A	4.59007	4.6024	-0.01233
20A	4.62342	4.94088	-0.31747
21A	4.64016	4.5603	0.079855
22A	4.8729	4.88582	-0.01292
23A	4.97469	4.99396	-0.01927
24A	4.42713	4.35755	0.069585
25A	4.16558	4.79791	-0.63233
26A	4.07779	4.04736	0.030429
27A	4.08302	4.0833	-0.00028
28A	4.11691	4.13672	-0.01981
29A	4.26043	4.26058	-0.00015
30A	4.33068	4.36286	-0.03218
31A	4.03058	4.04452	-0.01394

^a Compounds **11A–31A** were selected from a previous paper.³⁵

reasonable model, the preliminary biological results of the compounds discussed in this paper and the previous paper were used. The calculated pIC_{50} values ranged from 4.03 to 6.04.

As the model dataset, 31 compounds (Table 3) with IC_{50} s ranging from 0.6 to 93.2 μM for inhibiting telomerase were selected. The operation process can be found in the previous paper.³⁵

The correlation coefficient, r^2 , between the observed and predicted activity of the training set was found to be 0.987, whereas that of the test set was found to be 0.316, which proved that this QSAR model was acceptable. The predicted pIC_{50} values and residual errors of 31 compounds analyzed using this QSAR model are listed in Table 3. A plot of the observed pIC_{50} versus the predicted data is provided in Fig. 6.

Moreover, the molecules aligned with the iso-surfaces of the 3D-QSAR model coefficients on van der Waals grids (Fig. 7a) and electrostatic potential grids (Fig. 7b) are shown. According to the maps, a compound with a high positive charge and a small oxygen-bearing heterocyclic group could show higher activity, which confirms that the 1,3-benzodioxole group is a better choice than 1,4-benzodioxan or 1,5-benzodioxepine. Similarly, a

highly negative-charged R group would also help obtain good activity, which confirms that the methoxy substituent could be more effective. This conclusion was similar to our previous result;³⁵ thus, it proved that our drug structure modification was reasonable. Therefore, the data summarized above demonstrates that compound **10a** is the most potent telomerase inhibitor ($\text{IC}_{50} = 0.6 \mu\text{M}$) containing suitable substituents that resulted in outstanding activity.

3 Conclusion

In summary, a series of novel 4,5-dihydropyrazole derivatives containing an oxygen-bearing heterocycle group were prepared as potential telomerase inhibitors. The activity assay results showed that compound **10a** exhibited the most potent telomerase inhibitory activity and good activity against human gastric cancer cell SGC-7901. Flow cytometric analysis and western blot results showed that **10a** induced both apoptosis and autophagy. A docking simulation was performed to position **10a** into the active site of 3DU6. The results showed that compound **10a** could bind well with the telomerase active site and act as a telomerase inhibitor. A QSAR model was also built using the activity data and binding conformations to provide a reliable tool that enables the rational design of novel telomerase inhibitors. This model can be used to predict activity and guide further structure modifications.

4 Experimental section

4.1 Chemicals

All chemicals and reagents used in this study were of analytical grade. The reactions were monitored by thin layer chromatography (TLC) on Merck pre-coated silica GF254 plates. Melting points (uncorrected) were determined on an X-4 MP apparatus (Taike Corp., Beijing, China). ESI mass spectra were obtained on a Mariner System 5304 mass spectrometer, and ^1H NMR spectra were collected on a Bruker DPX300 spectrometer at room temperature using TMS and solvent signals as internal standards. Chemical shifts were reported in ppm (δ). Elemental analyses were performed on a CHN-O-Rapid instrument, and they were within $\pm 0.4\%$ of the theoretical values.

4.1.1 General synthetic procedure for compounds 1–3. In the three-necked flask under a nitrogen atmosphere, 3,4-dihydroxybenzaldehyde (0.828 g, 6 mmol) was dissolved in dry acetone (10 ml), and then anhydrous potassium carbonate (2.5 g) was added to the solution. After that, the acetone solution containing dibromomethane or 1,2-dibromoethane or 1,3-dibromopropane (6 mmol) was added dropwise and refluxed for 24 h. The reaction solution was evaporated using a reduced pressure distillation. An appropriate amount of water was added to the residue, and the resulting mixture was extracted with ethyl acetate ($3 \times 40 \text{ ml}$). The organic layers were combined and dried with anhydrous magnesium sulfate. The solvent was then removed under a reduced pressure steam to afford the crude product, which was purified by column chromatography [eluent: $v(\text{petroleum ether})/v(\text{ethyl acetate}) = 4 : 1$] to give a white coloured solid (compounds 1–3).

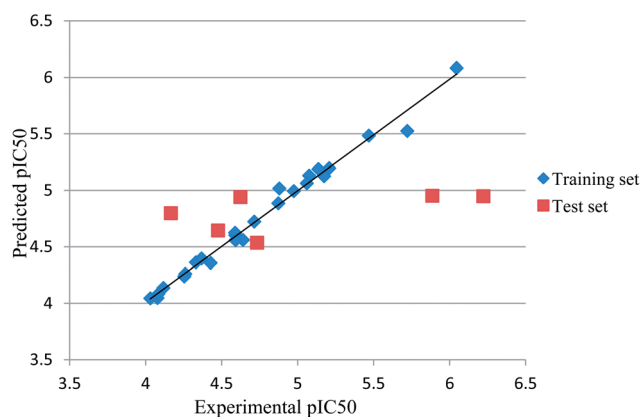


Fig. 6 Experimental versus predicted telomerase inhibitory activities of the training set and the test set.

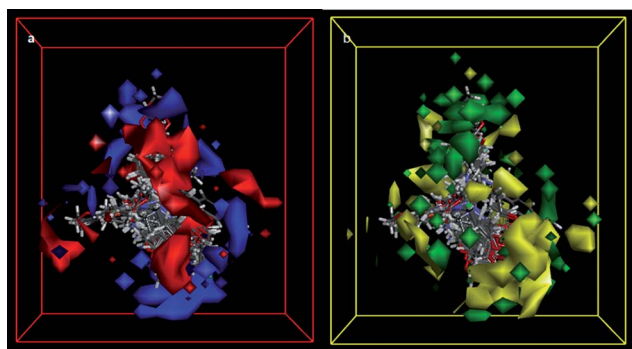


Fig. 7 (a) 3D-QSAR model coefficients on van der Waals grids. Green represents positive coefficients; yellow represents negative coefficients. (b) 3D-QSAR model coefficients on electrostatic potential grids. Blue represents positive coefficients; red represents negative coefficients.

4.1.2 General synthetic procedure for chalcones 10–27.

Equimolar portions of the synthesized compounds 1–3 (10 mmol) and substituted benzaldehydes 4–9 (10 mmol) were dissolved in approximately 15 ml of ethanol. The mixture was allowed to stir for several minutes at 5–10 °C. A 10 ml aliquot of a 40% aqueous potassium hydroxide solution was then slowly added dropwise to the reaction flask *via* a self-equalizing addition funnel. The reaction solution was allowed to stir at room temperature for approximately 4 h. Typically, after the completion of the reaction, a precipitate was formed, which was then collected by suction filtration.

4.1.3 (*E*)-3-(3,4-Dihydro-2*H*-benzo[*b*][1,4]dioxepin-7-yl)-1-phenylprop-2-en-1-one (22). White solid, yield: 25%. MP: 102–104 °C. ¹H NMR (CDCl₃, 300 MHz): 2.12 (s, 2H), 4.23 (m, 4H), 6.91–6.97 (m, 1H), 7.12–7.27 (m, 3H), 7.24 (dd, *J*₁ = 6.24 Hz, *J*₂ = 8.42 Hz, 1H), 7.29 (d, *J* = 2.19 Hz, 1H), 7.39 (d, *J* = 15.60 Hz, 1H), 7.63–8.07 (m, 3H). ESI-MS: 281.11 (C₁₈H₁₇O₃, [M + H]⁺). Anal. calcd for C₁₈H₁₆O₃: C, 77.12; H, 5.75%. Found: C, 77.10; H, 5.76%.

4.1.4 (*E*)-3-(3,4-Dihydro-2*H*-benzo[*b*][1,4]dioxepin-7-yl)-1-(4-fluorophenyl) prop-2-en-1-one (23). White solid, yield: 26%. MP: 107–110 °C. ¹H NMR (CDCl₃, 300 MHz): 2.11 (s, 2H), 4.20 (m, 4H), 6.90–6.99 (m, 1H), 7.13–7.20 (m, 3H), 7.23 (dd, *J*₁ = 6.21 Hz, *J*₂ = 8.43 Hz, 1H), 7.28 (d, *J* = 2.19 Hz, 1H), 7.36 (d, *J* = 15.54 Hz, 1H), 7.60–8.06 (m, 2H). ESI-MS: 299.31 (C₁₈H₁₆FO₃, [M + H]⁺). Anal. calcd for C₁₈H₁₅FO₃: C, 72.47; H, 5.07%. Found: C, 72.50; H, 5.06%.

4.1.5 (*E*)-1-(4-Chlorophenyl)-3-(3,4-dihydro-2*H*-benzo[*b*][1,4]-dioxepin-7-yl)prop-2-en-1-one (24). White solid, yield: 24%. MP: 113–115 °C. ¹H NMR (CDCl₃, 300 MHz): 2.11 (s, 2H), 4.17 (m, 4H), 7.02–7.04 (m, 1H), 7.11–7.15 (m, 3H), 7.21 (d, *J* = 10.22 Hz, 1H), 7.25 (d, *J* = 15.54 Hz, 1H), 7.44 (d, *J* = 15.84 Hz, 1H), 7.94–8.03 (m, 2H). ESI-MS: 314.76 (C₁₈H₁₆ClO₃, [M + H]⁺). Anal. calcd for C₁₈H₁₅ClO₃: C, 68.68; H, 4.80%. Found: C, 68.71; H, 4.82%.

4.1.6 (*E*)-1-(4-Bromophenyl)-3-(3,4-dihydro-2*H*-benzo[*b*][1,4]-dioxepin-7-yl)prop-2-en-1-one (25). White solid, yield: 28%. MP: 120–122 °C. ¹H NMR (DMSO-*d*₆, 300 MHz): 2.11 (s, 2H), 4.19 (m, 4H), 7.03 (d, *J* = 8.4 Hz, 1H), 7.47–7.50 (m, 1H), 7.63 (s, 1H), 7.72 (d, *J* = 15.54 Hz, 1H), 7.85 (d, *J* = 15.54 Hz, 1H), 8.21–8.40 (m, 4H). ESI-MS: 359.21 (C₁₈H₁₆BrO₃, [M + H]⁺). Anal. calcd for C₁₈H₁₅BrO₃: C, 60.18; H, 4.21%. Found: C, 60.20; H, 4.22%.

4.1.7 (*E*)-3-(3,4-Dihydro-2*H*-benzo[*b*][1,4]dioxepin-7-yl)-1-*p*-tolylprop-2-en-1-one (26). White solid, yield: 26%. MP: 99–101 °C. ¹H NMR (CDCl₃, 300 MHz): 2.11 (s, 2H), 2.45 (s, 3H), 4.26–4.32 (m, 4H), 6.93–7.01 (m, 1H), 7.21–7.24 (m, 1H), 7.25–7.29 (m, 3H), 7.31 (d, *J* = 3.23 Hz, 1H), 7.42 (d, *J* = 15.54 Hz, 1H), 7.62–7.95 (m, 2H). ESI-MS: 295.34 (C₁₉H₁₉O₃, [M + H]⁺). Anal. calcd for C₁₉H₁₈O₃: C, 77.53; H, 6.16%. Found: C, 77.56; H, 6.18%.

4.1.8 (*E*)-3-(3,4-Dihydro-2*H*-benzo[*b*][1,4]dioxepin-7-yl)-1-(4-methoxyphenyl) prop-2-en-1-one (27). White solid, yield: 30%. MP: 105–108 °C. ¹H NMR (CDCl₃, 300 MHz): 2.11 (s, 2H), 3.84 (s, 3H), 4.26 (d, *J* = 2.84 Hz, 4H), 6.94–7.02 (m, 1H), 7.23–7.25 (m, 1H), 7.27–7.31 (m, 3H), 7.35 (d, *J* = 3.63 Hz, 1H), 7.45 (d, *J* = 15.54 Hz, 1H), 7.62–7.95 (m, 2H). ESI-MS: 311.34 (C₁₉H₁₉O₄, [M + H]⁺). Anal. calcd for C₁₉H₁₈O₄: C, 73.53; H, 5.85%. Found: C, 73.51; H, 5.86%.

4.1.9 General synthetic procedure of dihydropyrazole derivatives 10a–27a. A mixture of chalcones 10–27 (10 mmol), thiosemicarbazide (10 mmol), and KOH (0.025 mol) was refluxed in ethanol (25 ml) for 12 h. The solution was poured into ice water. The precipitate was filtered and crystallized from methanol to afford the target compounds.

4.1.10 5-(Benzo[*d*][1,3]dioxol-5-yl)-3-phenyl-4,5-dihydro-1*H*-pyrazole-1-carbothioamide (10a). White crystal, yield: 75%. MP: 196–198 °C. ¹H NMR (DMSO-*d*₆, 300 MHz): 3.09–3.17 (m, 1H), 3.80–3.90 (m, 1H), 5.84 (dd, *J*₁ = 3.12 Hz, *J*₂ = 11.16 Hz, 1H), 5.97 (s, 2H), 6.59–6.65 (m, 2H), 6.84 (d, *J* = 7.86 Hz, 1H), 7.43–7.47 (m, 3H), 7.86–7.89 (m, 3H), 8.02 (s, 1H). ESI-MS: 326.38 (C₁₇H₁₆N₃O₂S, [M + H]⁺). Anal. calcd for C₁₇H₁₅N₃O₂S: C, 62.75; H, 4.65; N, 12.91%. Found: C, 62.72; H, 4.64; N, 12.89%.

4.1.11 5-(Benzo[*d*][1,3]dioxol-5-yl)-3-(4-fluorophenyl)-4,5-dihydro-1*H*-pyrazole-1-carbothioamide (11a). White crystal, yield: 72%. MP: 213–214 °C. ¹H NMR (DMSO-*d*₆, 300 MHz): 3.14 (dd, *J*₁ = 3.27 Hz, *J*₂ = 17.91, 1H), 3.84 (dd, *J*₁ = 11.13 Hz, *J*₂ = 17.91 Hz, 1H), 5.84 (d, *J* = 8.25 Hz, 1H), 5.97 (s, 2H), 6.59–6.64 (m, 2H), 6.84 (d, *J* = 7.89 Hz, 1H), 7.30 (t, *J* = 8.97 Hz, 2H), 7.91–7.96 (m, 3H), 8.02 (s, 1H). ESI-MS: 344.38 (C₁₇H₁₅FN₃O₂S, [M + H]⁺). Anal. calcd for C₁₇H₁₄FN₃O₂S: C, 59.46; H, 4.11; N, 12.24%. Found: C, 59.44; H, 4.12; N, 12.23%.

4.1.12 5-(Benzo[*d*][1,3]dioxol-5-yl)-3-(4-chlorophenyl)-4,5-dihydro-1*H*-pyrazole-1-carbothioamide (12a). White crystal, yield: 73%. MP: 221–223 °C. ¹H NMR (DMSO-*d*₆, 300 MHz): 3.13 (dd, *J*₁ = 3.48 Hz, *J*₂ = 18.12 Hz, 1H), 3.84 (dd, *J*₁ = 11.34 Hz, *J*₂ = 18.12 Hz, 1H), 5.84 (dd, *J*₁ = 3.48 Hz, *J*₂ = 11.34 Hz, 1H), 5.97 (s, 2H), 6.58–6.64 (m, 2H), 6.83 (d, *J* = 8.04 Hz, 1H), 7.52 (d, *J* = 8.58 Hz, 2H), 7.80 (d, *J* = 8.58 Hz, 2H), 7.81–7.90 (m, 1H), 8.05 (s, 1H). ESI-MS: 360.83 (C₁₇H₁₅ClN₃O₂S, [M + H]⁺). Anal. calcd for C₁₇H₁₄ClN₃O₂S: C, 56.74; H, 3.92; N, 11.68%. Found: C, 56.72; H, 3.91; N, 11.70%.

4.1.13 5-(Benzo[*d*][1,3]dioxol-5-yl)-3-(4-bromophenyl)-4,5-dihydro-1*H*-pyrazole-1-carbothioamide (13a). White crystal, yield: 69%. MP: 231–233 °C. ¹H NMR (DMSO-*d*₆, 300 MHz): 3.13 (dd, *J*₁ = 3.48 Hz, *J*₂ = 18.12 Hz, 1H), 3.84 (dd, *J*₁ = 11.34 Hz, *J*₂ = 17.98 Hz, 1H), 5.84 (d, *J* = 8.04 Hz, 1H), 5.97 (s, 2H), 6.59–6.65 (m, 2H), 6.84 (d, *J* = 8.04 Hz, 1H), 7.65 (d, *J* = 8.58 Hz, 2H), 7.82 (d, *J* = 8.61 Hz, 2H), 7.94 (s, 1H), 8.05 (s, 1H). ESI-MS: 405.28 (C₁₇H₁₅BrN₃O₂S, [M + H]⁺). Anal. calcd for C₁₇H₁₄BrN₃O₂S: C, 50.50; H, 3.49; N, 10.39%. Found: C, 50.52; H, 3.47; N, 10.42%.

4.1.14 5-(Benzo[*d*][1,3]dioxol-5-yl)-3-*p*-tolyl-4,5-dihydro-1*H*-pyrazole-1-carbothioamide (14a). White crystal, yield: 65%. MP: 202–204 °C. ¹H NMR (DMSO-*d*₆, 300 MHz): 2.34 (s, 3H), 3.10 (dd, *J*₁ = 3.30 Hz, *J*₂ = 18.12 Hz, 1H), 3.83 (dd, *J*₁ = 11.16 Hz, *J*₂ = 17.91 Hz, 1H), 5.83 (dd, *J*₁ = 3.12 Hz, *J*₂ = 11.16 Hz, 1H), 5.97 (s, 2H), 6.58–6.65 (m, 2H), 6.83 (d, *J* = 8.04 Hz, 1H), 7.26 (d, *J* = 8.10 Hz, 2H), 7.76 (d, *J* = 8.22 Hz, 2H), 7.82 (s, 1H), 7.97 (s, 1H). ESI-MS: 340.41 (C₁₈H₁₈N₃O₂S, [M + H]⁺). Anal. calcd for C₁₈H₁₇N₃O₂S: C, 63.70; H, 5.05; N, 12.38%. Found: C, 63.72; H, 5.04; N, 12.40%.

4.1.15 5-(Benzo[*d*][1,3]dioxol-5-yl)-3-(4-methoxyphenyl)-4,5-dihydro-1*H*-pyrazole-1-carbothioamide (15a). White crystal, yield: 73%. MP: 210–212 °C. ¹H NMR (DMSO-*d*₆, 300 MHz): 3.10 (d, *J* = 13.64 Hz, 1H), 3.83 (m, 4H), 5.81 (d, *J* = 8.04 Hz, 1H), 5.96

(s, 2H), 6.61 (t, $J = 7.77$ Hz, 2H), 6.82 (d, $J = 8.07$ Hz, 1H), 7.00 (d, $J = 8.97$ Hz, 2H), 7.81 (d, $J = 8.76$ Hz, 2H), 7.92 (s, 1H). ESI-MS: 356.41 ($C_{18}H_{18}N_3O_3S$, $[M + H]^+$). Anal. calcd for $C_{18}H_{17}N_3O_3S$: C, 60.83; H, 4.82; N, 11.82%. Found: C, 60.81; H, 4.81; N, 11.85%.

4.1.16 5-(2,3-Dihydrobenzo[*b*][1,4]dioxin-6-yl)-3-phenyl-4,5-dihydro-1H-pyrazole-1-carbothioamide (16a). White crystal, yield: 57%. MP: 198–200 °C. 1H NMR (DMSO- D_6 , 300 MHz): 3.12 (dd, $J_1 = 3.09$ Hz, $J_2 = 17.91$ Hz, 1H), 3.83 (dd, $J_1 = 11.16$ Hz, $J_2 = 17.94$ Hz, 1H), 4.22 (d, $J = 20.49$ Hz, 4H), 5.81 (dd, $J_1 = 3.12$ Hz, $J_2 = 11.16$ Hz, 1H), 6.58–6.61 (m, 2H), 6.78 (d, $J = 8.04$ Hz, 1H), 7.41–7.47 (m, 3H), 7.86–7.89 (m, 3H), 8.00 (s, 1H). ESI-MS: 340.41 ($C_{18}H_{18}N_3O_2S$, $[M + H]^+$). Anal. calcd for $C_{18}H_{17}N_3O_2S$: C, 63.70; H, 5.05; N, 12.38%. Found: C, 63.72; H, 5.04; N, 12.37%.

4.1.17 5-(2,3-Dihydrobenzo[*b*][1,4]dioxin-6-yl)-3-(4-fluorophenyl)-4,5-dihydro-1H-pyrazole-1-carbothioamide (17a). White crystal, yield: 74%. MP: 205–207 °C. 1H NMR (DMSO- D_6 , 300 MHz): 3.10 (dd, $J_1 = 3.27$ Hz, $J_2 = 18.09$ Hz, 1H), 3.80 (dd, $J_1 = 11.34$ Hz, $J_2 = 18.12$ Hz, 1H), 4.17 (s, 4H), 5.79 (dd, $J_1 = 3.09$ Hz, $J_2 = 11.31$ Hz, 1H), 6.55–6.59 (m, 2H), 6.76 (d, $J = 7.86$ Hz, 1H), 7.28 (t, $J = 8.96$ Hz, 2H), 7.89–7.99 (m, 4H). ESI-MS: 358.40 ($C_{18}H_{17}FN_3O_2S$, $[M + H]^+$). Anal. calcd for $C_{18}H_{16}FN_3O_2S$: C, 60.49; H, 4.51; N, 11.76%. Found: C, 60.51; H, 4.50; N, 11.78%.

4.1.18 3-(4-Chlorophenyl)-5-(2,3-dihydrobenzo[*b*][1,4]dioxin-6-yl)-4,5-dihydro-1H-pyrazole-1-carbothioamide (18a). White crystal, yield: 76%. MP: 225–226 °C. 1H NMR (DMSO- D_6 , 300 MHz): 3.11 (dd, $J_1 = 3.12$ Hz, $J_2 = 17.70$ Hz, 1H), 3.82 (dd, $J_1 = 11.34$ Hz, $J_2 = 18.09$ Hz, 1H), 4.19 (s, 4H), 5.81 (dd, $J_1 = 3.12$ Hz, $J_2 = 11.34$ Hz, 1H), 6.57–6.60 (m, 2H), 6.77 (d, $J = 8.25$ Hz, 1H), 7.52 (dd, $J_1 = 2.01$ Hz, $J_2 = 6.75$ Hz, 2H), 7.88–7.90 (m, 2H), 7.92 (d, $J = 7.68$ Hz, 1H), 8.03 (s, 1H). ESI-MS: 374.86 ($C_{18}H_{17}ClN_3O_2S$, $[M + H]^+$). Anal. calcd for $C_{18}H_{16}ClN_3O_2S$: C, 57.83; H, 4.31; N, 11.24%. Found: C, 57.81; H, 4.30; N, 11.22%.

4.1.19 3-(4-Bromophenyl)-5-(2,3-dihydrobenzo[*b*][1,4]dioxin-6-yl)-4,5-dihydro-1H-pyrazole-1-carbothioamide (19a). White crystal, yield: 64%. MP: 236–238 °C. 1H NMR (DMSO- D_6 , 300 MHz): 3.10 (dd, $J_1 = 3.48$ Hz, $J_2 = 18.09$ Hz, 1H), 3.81 (dd, $J_1 = 11.16$ Hz, $J_2 = 17.73$ Hz, 1H), 4.19 (s, 4H), 5.81 (d, $J = 8.22$ Hz, 1H), 6.57–6.60 (m, 2H), 6.77 (d, $J = 8.04$ Hz, 1H), 7.65 (d, $J = 8.61$ Hz, 2H), 7.80–7.93 (m, 2H), 8.04 (s, 1H), 8.31 (s, 1H). ESI-MS: 419.31 ($C_{18}H_{17}BrN_3O_2S$, $[M + H]^+$). Anal. calcd for $C_{18}H_{16}BrN_3O_2S$: C, 51.68; H, 3.86; N, 10.05%. Found: C, 51.70; H, 3.85; N, 10.06%.

4.1.20 5-(2,3-Dihydrobenzo[*b*][1,4]dioxin-6-yl)-3-*p*-tolyl-4,5-dihydro-1H-pyrazole-1-carbothioamide (20a). White crystal, yield: 75%. MP: 203–205 °C. 1H NMR (DMSO- D_6 , 300 MHz): 2.34 (s, 3H), 3.08 (dd, $J_1 = 2.94$ Hz, $J_2 = 17.91$ Hz, 1H), 3.80 (dd, $J_1 = 11.16$ Hz, $J_2 = 17.76$ Hz, 1H), 4.19 (s, 4H), 5.80 (dd, $J_1 = 3.09$ Hz, $J_2 = 11.13$ Hz, 1H), 6.56–6.60 (m, 2H), 6.77 (d, $J = 8.04$ Hz, 1H), 7.26 (d, $J = 8.04$ Hz, 2H), 7.76 (d, $J = 8.22$ Hz, 2H), 7.81 (s, 1H), 7.96 (s, 1H). ESI-MS: 354.44 ($C_{19}H_{20}N_3O_2S$, $[M + H]^+$). Anal. calcd for $C_{19}H_{19}N_3O_2S$: C, 64.57; H, 5.42; N, 11.89%. Found: C, 64.55; H, 5.41; N, 11.87%.

4.1.21 5-(2,3-Dihydrobenzo[*b*][1,4]dioxin-6-yl)-3-*p*-tolyl-4,5-dihydro-1H-pyrazole-1-carbothioamide (21a). White crystal, yield: 78%. MP: 212–214 °C. 1H NMR (DMSO- D_6 , 300 MHz): 3.08 (dd, $J_1 = 2.94$ Hz, $J_2 = 17.96$ Hz, 1H), 3.79 (dd, $J_1 = 11.52$ Hz, $J_2 = 19.20$ Hz, 1H), 3.83 (s, 3H), 4.19 (s, 4H), 5.79 (d, $J = 8.22$ Hz, 1H),

6.58 (d, $J = 8.61$ Hz, 2H), 6.77 (d, $J = 8.04$ Hz, 1H), 7.00 (d, $J = 8.76$ Hz, 2H), 7.81 (d, $J = 8.79$ Hz, 3H), 7.91 (s, 1H). ESI-MS: 370.44 ($C_{19}H_{20}N_3O_3S$, $[M + H]^+$). Anal. calcd for $C_{19}H_{19}N_3O_3S$: C, 61.77; H, 5.18; N, 11.37%. Found: C, 61.76; H, 5.17; N, 11.36%.

4.1.22 5-(3,4-Dihydro-2H-benzo[*b*][1,4]dioxepin-7-yl)-3-phenyl-4,5-dihydro-1H-pyrazole-1-carbothioamide (22a). White crystal, yield: 67%. MP: 201–203 °C. 1H NMR (DMSO- D_6 , 300 MHz): 2.10 (s, 2H), 3.12 (dd, $J_1 = 3.02$ Hz, $J_2 = 17.98$ Hz, 1H), 3.84 (dd, $J_1 = 11.34$ Hz, $J_2 = 18.02$ Hz, 1H), 4.13 (s, 4H), 5.86 (dd, $J_1 = 2.96$ Hz, $J_2 = 11.24$ Hz, 1H), 6.72 (d, $J = 8.01$ Hz, 2H), 6.86–6.98 (m, 2H), 7.34 (t, $J = 8.78$ Hz, 2H), 7.80–8.05 (m, 4H), 8.03 (s, 1H). ESI-MS: 354.12 ($C_{19}H_{20}N_3O_2S$, $[M + H]^+$). Anal. calcd for $C_{19}H_{19}N_3O_2S$: C, 64.57; H, 5.42; N, 11.89%. Found: C, 61.47; H, 4.87; N, 11.32%.

4.1.23 5-(3,4-Dihydro-2H-benzo[*b*][1,4]dioxepin-7-yl)-3-(4-fluorophenyl)-4,5-dihydro-1H-pyrazole-1-carbothioamide (23a). White crystal, yield: 72%. MP: 207–210 °C. 1H NMR (DMSO- D_6 , 300 MHz): 2.11 (s, 2H), 3.13 (dd, $J_1 = 2.94$ Hz, $J_2 = 17.94$ Hz, 1H), 3.82 (dd, $J_1 = 11.24$ Hz, $J_2 = 17.87$ Hz, 1H), 4.14 (s, 4H), 5.84 (dd, $J_1 = 2.94$ Hz, $J_2 = 11.16$ Hz, 1H), 6.70 (d, $J = 8.04$ Hz, 2H), 6.87–6.97 (m, 1H), 7.30 (t, $J = 8.78$ Hz, 2H), 7.78–8.01 (m, 4H). ESI-MS: 372.43 ($C_{19}H_{19}FN_3O_2S$, $[M + H]^+$). Anal. calcd for $C_{19}H_{18}FN_3O_2S$: C, 61.44; H, 4.88; N, 11.31%. Found: C, 61.47; H, 4.87; N, 11.32%.

4.1.24 3-(4-Chlorophenyl)-5-(3,4-dihydro-2H-benzo[*b*][1,4]dioxepin-7-yl)-4,5-dihydro-1H-pyrazole-1-carbothioamide (24a). White crystal, yield: 78%. MP: 220–222 °C. 1H NMR (DMSO- D_6 , 300 MHz): 2.06 (s, 2H), 3.11 (dd, $J_1 = 3.09$ Hz, $J_2 = 17.91$ Hz, 1H), 3.81 (dd, $J_1 = 11.16$ Hz, $J_2 = 17.94$ Hz, 1H), 4.08 (s, 4H), 5.82 (d, $J = 8.25$ Hz, 1H), 6.67–6.70 (m, 2H), 6.88 (d, $J = 8.40$ Hz, 1H), 7.50 (d, $J = 8.43$ Hz, 2H), 7.86–7.89 (m, 2H), 7.92 (s, 1H), 8.03 (s, 1H). ESI-MS: 388.88 ($C_{19}H_{19}ClN_3O_2S$, $[M + H]^+$). Anal. calcd for $C_{19}H_{18}ClN_3O_2S$: C, 58.83; H, 4.68; N, 10.83%. Found: C, 58.81; H, 4.67; N, 10.81%.

4.1.25 3-(4-Bromophenyl)-5-(3,4-dihydro-2H-benzo[*b*][1,4]dioxepin-7-yl)-4,5-dihydro-1H-pyrazole-1-carbothioamide (25a). White crystal, yield: 71%. MP: 226–228 °C. 1H NMR (DMSO- D_6 , 300 MHz): 2.08 (s, 2H), 3.12 (dd, $J_1 = 3.30$ Hz, $J_2 = 18.12$ Hz, 1H), 3.83 (dd, $J_1 = 11.34$ Hz, $J_2 = 18.09$ Hz, 1H), 4.08 (s, 4H), 5.85 (dd, $J_1 = 3.09$ Hz, $J_2 = 11.34$ Hz, 1H), 6.68–6.72 (m, 2H), 6.89 (d, $J = 7.86$ Hz, 1H), 7.65 (d, $J = 8.58$ Hz, 2H), 7.82 (d, $J = 8.40$ Hz, 2H), 7.95 (s, 1H), 8.06 (s, 1H). ESI-MS: 433.33 ($C_{19}H_{19}BrN_3O_2S$, $[M + H]^+$). Anal. calcd for $C_{19}H_{18}BrN_3O_2S$: C, 52.78; H, 4.20; N, 9.72%. Found: C, 52.80; H, 4.21; N, 9.74%.

4.1.26 5-(3,4-Dihydro-2H-benzo[*b*][1,4]dioxepin-7-yl)-3-*p*-tolyl-4,5-dihydro-1H-pyrazole-1-carbothioamide (26a). White crystal, yield: 69%. MP: 202–205 °C. 1H NMR (DMSO- D_6 , 300 MHz): 2.07 (s, 2H), 2.34 (s, 3H), 3.10 (dd, $J_1 = 3.09$ Hz, $J_2 = 17.91$ Hz, 1H), 3.81 (dd, $J_1 = 11.16$ Hz, $J_2 = 17.91$ Hz, 1H), 4.09 (s, 4H), 5.83 (d, $J = 8.22$ Hz, 1H), 6.68–6.72 (m, 2H), 6.89 (d, $J = 8.04$ Hz, 1H), 7.26 (d, $J = 7.86$ Hz, 2H), 7.76 (d, $J = 8.07$ Hz, 2H), 7.83 (s, 1H), 7.97 (s, 1H). ESI-MS: 368.46 ($C_{20}H_{22}N_3O_2S$, $[M + H]^+$). Anal. calcd for $C_{20}H_{21}N_3O_2S$: C, 65.37; H, 5.76; N, 11.44%. Found: C, 65.35; H, 5.75; N, 11.46%.

4.1.27 5-(3,4-Dihydro-2H-benzo[*b*][1,4]dioxepin-7-yl)-3-(4-methoxyphenyl)-4,5-dihydro-1H-pyrazole-1-carbothioamide (27a). White crystal, yield: 64%. MP: 214–217 °C. 1H NMR (DMSO- D_6 , 300 MHz): 2.08 (s, 2H), 3.10 (dd, $J_1 = 3.16$ Hz, $J_2 = 18.04$ Hz, 1H),

3.80 (dd, $J_1 = 11.24$ Hz, $J_2 = 18.04$ Hz, 1H), 3.84 (s, 3H), 4.11 (s, 4H), 5.83 (d, $J = 8.14$ Hz, 1H), 6.68–6.71 (m, 2H), 6.85 (d, $J = 8.12$ Hz, 1H), 7.34 (d, $J = 8.34$ Hz, 2H), 7.78 (d, $J = 7.94$ Hz, 2H), 7.83 (s, 1H), 7.95 (s, 1H). ESI-MS: 384.46 ($C_{20}H_{22}N_3O_3S$, $[M + H]^+$). Anal. calcd for $C_{20}H_{22}N_3O_3S$: C, 62.64; H, 5.52; N, 10.96%. Found: C, 62.66; H, 5.53; N, 10.97%.

4.2 Biology

4.2.1 Telomerase inhibition assay. Compounds **10a–27a** were assayed for telomerase inhibition by a modified TRAP assay with a SGC-7901 cell extract. The telomerase assay methods used are the same as those previously described.³⁴ The results are reported in Table 1.

4.2.2 Antiproliferative activity assay. The antiproliferative activity of the prepared compounds **10a–27a** against SGC-7901 and B16-F10 cells was evaluated by the following protocol. Target tumor cells were grown to log phase in RPMI 1640 medium supplemented with 10% fetal bovine serum. After reaching a dilution of 3×10^4 cells per ml in the medium, 100 μ l of the obtained cell suspension was added to each well of a 96-well culture plate. Subsequently, incubation was performed at 37 °C in 5% CO₂ atmosphere for 24 h before the cytotoxicity assessment. Tested samples at pre-set concentrations were added to six wells with 5-fluorouracil employed as a positive reference. After a 48 h exposure period, 25 μ l of PBS containing 2.5 mg ml⁻¹ of MTT was added to each well. After 4 h, the medium was replaced with 150 μ l DMSO to dissolve the purple formazan crystals produced. The absorbance at 570 nm of each well was measured using an ELISA plate reader. The data are represented as a mean of three independent experiments performed in triplicate and are expressed as mean \pm SD. The IC₅₀ value was defined as the concentration, at which 50% of the cells survived. The results are summarized in Table 2.

4.2.3 Flow cytometry assay. SGC-7901 cells were seeded into T25 culture flasks and treated the following day with 3 μ M concentrations of test compounds for 72 h or left untreated (control condition). Each sample was evaluated in triplicate. The samples were then analyzed by FACS Calibur flow cytometer (Becton Dickinson, San Jose, CA).

4.2.4 Western blot analysis. After incubation for 24 h, the SGC-7901 cells were washed with PBS and lysed in the lysis buffer (30 mM Tris, pH 7.5, 150 mM sodium chloride, 1 mM phenylmethylsulfonyl fluoride, 1 mM sodium orthovanadate, 1% Nonidet P-40, 10% glycerol, and phosphatase and protease inhibitors). After 10 000g centrifugation for 10 min, the protein content of the supernatant was determined by a BCATM protein assay kit (Pierce, Rockford, IL). The protein lysates were separated by 10% SDS-PAGE and subsequently electrotransferred onto a polyvinylidene difluoride membrane (Millipore Corp., Bedford, MA). The membrane was blocked with 5% non-fat milk for 2 h at room temperature. The blocked membrane was probed with the indicated primary antibodies overnight at 4 °C, and then incubated with a horse radish peroxidase (HRP)-coupled secondary antibody. The detection was performed using a LumiGLO chemiluminescent substrate system (KPL, Guildford, UK).

4.3 Docking simulations

Molecular docking of compounds **10a** into the three-dimensional X-ray structure of telomerase catalytic subunit (PDB code: 3DU6) was carried out using the Discovery Studio (version 3.5) as implemented using Discovery Studio CDOCKER protocol.

The three-dimensional structures of the aforementioned compounds were constructed using ChemBio 3D Ultra 11.0 software [Chemical Structure Drawing Standard; Cambridge Soft corporation, USA (2008)], and then they were energetically minimized using MMFF94 with 5000 iterations and a minimum RMS gradient of 0.10. The crystal structures of TERT protein catalytic subunit were retrieved from the RCSB Protein Data Bank (<http://www.rcsb.org/pdb/home/home.-do>). All bound water and ligands were eliminated from the protein and polar hydrogens were added. The whole 3DU6 was defined as a receptor, and the site sphere was selected based on the active centre of 3DU6 according to a previous report.⁵ Subsequently, compound **10a** was placed in the molecular docking procedure, and different types of interactions between the docked protein and the ligand were analyzed at the end of the molecular docking.

4.4 QSAR model

A subset of 25 compounds was utilized as a training set for QSAR modeling. Because it is essential to assess the predictive power of the resulting QSAR models on an external set of inhibitors, the remaining 4 molecules (*ca.* 20% of the dataset) were employed as an external test subset for validating the QSAR models by the Diverse Molecules protocol in the Discovery Studio 3.1. The selected test compounds were: **20A**, **10a**, **25A**, **15A**, **18A** and **17a**.

The inhibitory ability of the compounds observed in the literature [IC₅₀ (mol l⁻¹)] was changed to a negative logarithmic scale [pIC₅₀ (mol l⁻¹)], and then used for subsequent QSAR analyses as a response variable.

In the Discovery Studio 3.1, the CHARMM force field was used and the electrostatic potential and the van der Waals potential were treated as separate terms. A +1e point charge was used as the electrostatic potential probe and the distance-dependent dielectric constant was used to mimic the solvation effect. For the van der Waals potential, a carbon atom with a radius of 1.73 Å was used as a probe. The truncation for both steric and the electrostatic energies was set to 30 kcal mol⁻¹. Standard parameters were implemented in the Discovery Studio 3.1.

A partial least-squares (PLS) model was built using energy grids as descriptors. QSAR models were built using the 3D-QSAR protocol of Discovery Studio 3.5.

Declaration

The content of the manuscript is original and has not been submitted for publication elsewhere. There is no conflict of interest in the manuscript. The main work on the synthesis of target compounds, evaluation of their biological activities, data analysis, and manuscript preparation were performed by Yin

Luo and Yang Zhou. Jie Fu contributed to the synthesis, biological assay, and data analysis. Hai-Liang Zhu is the corresponding author.

Acknowledgements

This work was supported by Jiangsu Planned Projects for Postdoctoral Research Funds (1302007C), China Postdoctoral Science Foundation Funds (2012M510131), International Postdoctoral Exchange Fellowship Program (20130023), National Undergraduate Innovation Program and the National Natural Science Foundation of China (No. J1103512, No. J1210026), and supported by "PCSIRT" (IRT1020).

References

- 1 B. Leber, C. M. Counter, C. B. Harley and S. Bacchetti, *Blood*, 1994, **84**, 10–19.
- 2 J. W. Shay and S. Bacchetti, *Eur. J. Cancer*, 1997, **33**, 787–791.
- 3 W. E. Wright and J. W. Shay, *Curr. Opin. Genet. Dev.*, 2001, **11**, 98–103.
- 4 A. G. Bodnar, M. Ouellette, M. Frolkis, S. E. Holt, C. P. Chiu, *et al.*, *Science*, 1998, **279**, 349–352.
- 5 A. J. Gillis, A. P. Schuller and E. Skordalakes, *Nature*, 2008, **455**, 633–637.
- 6 C. B. Harley, N. W. Kim, K. R. Prowse, S. L. Weinrich, K. S. Hirsch, M. D. West, *et al.*, *Cold Spring Harbor Symposia On Quantitative Biology*, 1994, **59**, 307–315.
- 7 M. Mason, A. Schuller and E. Skordalakes, *Curr. Opin. Struct. Biol.*, 2011, **21**, 92–100.
- 8 C. Philippi, B. Loretz, U. F. Schaefer and C. M. Lehr, *J. Controlled Release*, 2010, **146**, 228–240.
- 9 J. H. Lee and I. K. Chung, *Cancer Lett.*, 2010, **290**, 76–86.
- 10 S. Kumar, S. Bawa, S. Drabu, R. Kumar and H. Gupta, *Recent Pat. Anti-Infect. Drug Discovery*, 2009, **4**, 154–163.
- 11 J. H. M. Lange and V. B. J. Vliet, Patent WO2010003760, 2010.
- 12 P. J. Coleman and C. D. Cox, Patent US2009042966, 2009.
- 13 M. Jeske and I. Flamme, Patent DE102007048447, 2009.
- 14 J. D. Kim, H. C. Yoon and I. W. Kin, Patent WO2006080821, 2007.
- 15 W. I. I. Bakker, J. Venhorst and A. V. Loevezijn, Patent AU2009226956, 2009.
- 16 B. S. Bhandodkar and S. Schmitt, Patent US2010179161, 2010.
- 17 S. Yenes-Minguez, A. Torrens-Jover and L. D. Esteve, Patent US2010099712, 2010.
- 18 A. H. Banday, B. P. Mir, I. H. Lone, K. A. Suri and H. M. Kumar, *Steroids*, 2010, **75**, 805–809.
- 19 F. Hayat, A. Salahuddin, S. Umar and A. Azam, *Eur. J. Med. Chem.*, 2010, **45**, 4669–4675.
- 20 K. S. Girisha, B. Kalluraya, V. Narayana and Padmashree, *Eur. J. Med. Chem.*, 2010, **45**, 4640–4644.
- 21 A. A. Bekhita and T. Abdel-Aziem, *Bioorg. Med. Chem.*, 2004, **12**, 1935–1945.
- 22 A. B. Need, R. J. Davis, J. T. Alexander-Chacko, B. Eastwood, E. Chernet, L. A. Phebus, D. K. Sindelar and G. G. Nomikos, *Psychopharmacology*, 2006, **184**, 26–35.
- 23 H. Dmytro, Z. Borys, V. Olexandr, Z. Lucjusz, G. Andrzej and L. Roman, *Eur. J. Med. Chem.*, 2009, **44**, 1396–1404.
- 24 X. H. Liu, H. F. Liu, X. Shen, B. A. Song, *et al.*, *Bioorg. Med. Chem. Lett.*, 2010, **20**, 4163–4167.
- 25 X. H. Liu, B. F. Ruan, J. X. Liu, B. A. Song, *et al.*, *Bioorg. Med. Chem. Lett.*, 2011, **21**, 2916–2920.
- 26 X. H. Liu, X. F. Liu, J. Chen, *et al.*, *Bioorg. Med. Chem. Lett.*, 2010, **20**, 5705–5708.
- 27 G. Altiokka and Z. Atkosar, *J. Pharm. Biomed. Anal.*, 2002, **27**, 841–844.
- 28 M. T. Vzquez, G. Rosell and M. D. Pujol, *Farmaco*, 1996, **51**, 215–217.
- 29 Y. Takano, M. Takano and T. L. Yaksh, *Eur. J. Pharmacol.*, 1992, **219**, 465–468.
- 30 A. Foroumadi, S. Mansouri, Z. Kiani and A. Rahmani, *Eur. J. Med. Chem.*, 2003, **38**, 851–854.
- 31 H. N. Dogan, A. Duran, S. Rollas, G. Sener, M. K. Uysal and D. Gülen, *Bioorg. Med. Chem.*, 2002, **10**, 2893–2898.
- 32 N. W. Kim, M. A. Piatyszek, K. R. Prowse, C. B. Harley, M. D. West, P. L. Ho, G. M. Coviello, W. E. Wright, S. L. Weinrich and J. W. Shay, *Science*, 1994, **266**, 2011–2015.
- 33 H. Han, L. H. Hurly and M. Salazar, *Nucleic Acids Res.*, 1999, **27**, 537–542.
- 34 N. W. Kim, M. A. Piatyszek, K. R. Prowse, C. B. Harley, M. D. West, P. L. C. Ho, G. M. Coviello, W. E. Wright, S. L. Weinrich and J. W. Shay, *Science*, 1994, **266**, 2011–2015.
- 35 Y. Luo, S. Zhang, K. M. Qiu, Z. J. Liu, Y. S. Yang, J. Fu, W. Q. Zhong and H. L. Zhu, *Bioorg. Med. Chem. Lett.*, 2013, **23**, 1091–1095.